

# **Microstructural Characterization and Modeling of Beam Speed Effects on Ti-6Al-4V by Electron Beam Additive Manufacturing**

X. Gong<sup>\*</sup>, J. Lydon<sup>†</sup>, K. Cooper<sup>†</sup>, and K. Chou<sup>\*</sup>

<sup>\*</sup>Mechanical Engineering Department

The University of Alabama  
Tuscaloosa, AL 35487

<sup>†</sup>Nonmetallic Branch  
Marshall Space Flight Center  
Huntsville, AL 35812

REVIEWED

## **Abstract**

In this study, the influence of the beam scanning speed to the microstructure of Ti-6Al-4V parts processed by EBAM is investigated. EBAM parts were fabricated with 4 different scanning speeds, ranging from 214 mm/s to 689 mm/s, and the microstructures were studied. In addition, the volume fractions of different phases were obtained by thermal and phase transformation modeling. The microstructure is characterized by columnar structures of prior  $\beta$  grains along the build direction, and fine Widmanstätten ( $\alpha+\beta$ ) structure and  $\alpha'$  martensites are presented inside of the prior  $\beta$ . Both the prior  $\beta$  grain size and  $\alpha$ -lath thickness decrease with the increase of the scanning speed. For the phase constitution, the volume fraction of  $\alpha'$  increases with the scanning speed while the volume fraction of  $\alpha$  decreases due to the increase of cooling rate during solid phase transformation. The results from the analytical phase transformation model are consistent with the microstructure characterization from the experiment.

## **Introduction**

Additive Manufacturing (AM), based on “layer-by-layer” fabrications, is an emerging technology, by which a physical solid part is made directly using electronic data of the part geometry. The powder-bed electron beam additive manufacturing (EBAM), using an electron beam to melt and fuse powder, is one of a few AM technologies for direct digital manufacturing of metal products [1]. Because of several unique advantages such as high energy efficiency, rapid scan speed, and moderate operation cost, etc., EBAM has attracted ever increasing interest from aerospace, military and biomedical industries, etc. Research subjects in EBAM have spread across a wide spectrum ranging from material and microstructural characterization [1,2], process modeling and simulation [3,4], process metrology [5], and geometric attributes [6,7], etc. Even with many advantages over conventional manufacturing technologies, EBAM still faces several challenges such as part accuracy and property value scattering.

Ti-6Al-4V is one of the most commonly used alloys in EBAM. Microstructures of Ti-6Al-4V samples from EBAM contain a mixture of phases such as Widmanstätten ( $\alpha+\beta$ ) and  $\alpha'$  martensite. The columnar prior  $\beta$  structure formed during initial solidification is generally noted, which is a result of very high temperature gradients, typically along the build direction [8,9]. Safdar et al. [9] reported typical ( $\alpha+\beta$ ) inside of the prior  $\beta$  grains. Facchini et al. [10] investigated microstructures of EBAM Ti-6Al-4V and showed that the main constituent is  $\alpha$  with

only a small fraction of  $\beta$  located at  $\alpha$ - $\alpha$  boundaries. Compared to the coarse ( $\alpha$ + $\beta$ ) shown in a cast specimen, the EBAM Ti-6Al-4V microstructure consists of fine ( $\alpha$ + $\beta$ ) and thin prior  $\beta$  grain boundaries [11]. Due to high cooling rates during solidification in EBAM,  $\alpha'$ -martensitic are present in the EBAM parts, which may contribute to increased strength and hardness, but lower ductility [12,13]. In summary, Ti-6Al-4V samples from EBAM have a fine Widmanstätten ( $\alpha$ + $\beta$ ) microstructure combined with  $\alpha'$ . However, it is expected that the microstructures of EBAM Ti-6Al-4V will vary with the process conditions.

It has been reported that EBAM process parameters may have significant effects on the part quality [14,15]. Murr et al. [14] reported that the variations in melt scan, beam current, and scan speed affect EBAM built defects such as porosity [16]. The beam scanning speed is one of major parameters in EBAM that affects the process condition [3]. It was reported that a higher scanning speed results in a greater cooling rate [17]. In a study conducted by Bontha et al. [15], it was suggested that increasing the scanning speed may result in a predominant decrease in the grain size of Ti-6Al-4V build parts. Despite of research on modeling and experiments of EBAM, there have been very few systematic studies on the relationship between the scanning speed and the microstructure of EBAM parts. In addition, there seems to be no research about quantitative studies of different phases in EBAM Ti-6Al-4V parts. Understanding the composition of different phases will offer insight for the study of the phase transformation and mechanical properties.

The objective of this study is to better understand the microstructural variations in EBAM built Ti-6Al-4V quantitatively. Specimens with different speed functions (related to the beam scanning speed) were fabricated. Moreover, the spatial distribution of the phase constitution is obtained by coupled thermal and phase transformation kinetic modeling. The intent is to correlate the EBAM Ti-6Al-4V microstructures with the process thermal characteristics.

### **Experimental Procedures**

An Arcam S12 EBAM machine at Marshall Space Flight Center was used to fabricate samples: 60 mm long, 5.5 mm wide and 25 mm high, using Ti-6Al-4V powder. For Arcam EBAM systems, the speed function (SF) is a setting related to the actual beam scanning speed [18]. In this study, four different SFs were tested (20, 36, 50 and 65) to investigate the beam speed effects on build part microstructures. The detailed information about the fabrication process can be found from a previous publication [19]. Figure 1 shows the EBAM fabricated samples processed with the corresponding speed function values. Fabricated Ti-6Al-4V samples were prepared for microstructural observations using common metallographic procedures. Specimens close to the top surface of the build parts were used for analysis. Specimens of different cross-sections (scanning surface: Z-plane, build side surface: X-plane) were prepared to examine the anisotropic conditions. To reveal the detailed microstructures, polished specimens were then etched with a hydrofluoric acid-based solution [14]. The etched metallographic samples were examined using a Leitz optical microscope (OM) and a Philips XL-30 scanning electron microscope (SEM). In order to quantify the size of columnar  $\beta$ , equiaxed  $\beta$  and  $\alpha$ -lath, a measurement method, from Wang et al [20], was employed. On the other hand, the analysis of the phase volume fractions ( $\alpha$ ,  $\beta$  and  $\alpha'$ ) was conducted using the square grid method [21].

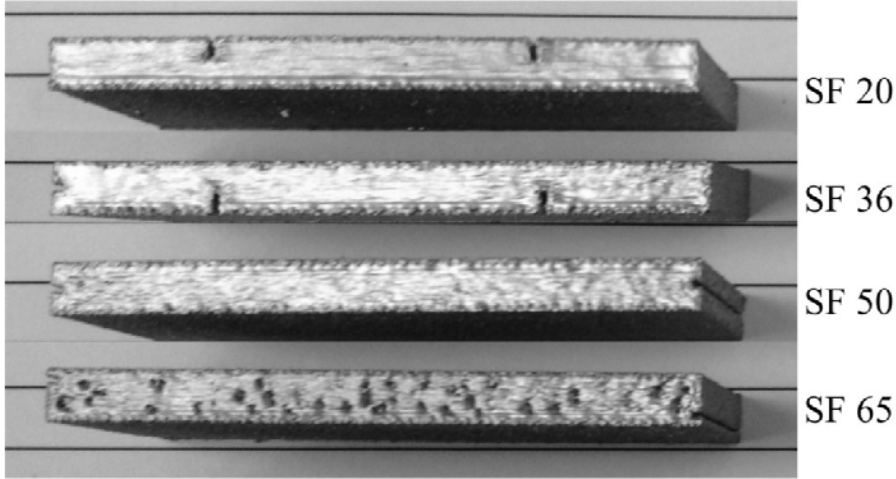


Figure 1. EBAM parts built with different speed function values.

## Results and Discussion

### Microstructures

Figure 2 shows typical microstructures from the X-plane of an EBAM sample, SF 36. It is obvious that the prior  $\beta$  grains grow along the build direction and across multiple layers in the sample. The solidification of Ti-6Al-4V alloy involves two steps: liquid to primary solid phase of  $\beta$  and solid phase transformation ( $\beta$  to  $\alpha$  or  $\alpha'$ ) depending on the cooling rate. The columnar prior  $\beta$  grains are typical in high-energy materials processing, and upon rapid cooling from the melt, the growing grains align themselves with the steepest temperature gradients [22] and result in columnar shaped morphology [23]. Another feature in typical EBAM Ti-6Al-4V microstructures is the martensitic phase,  $\alpha'$ , which appears as plates, as can be seen in Figure 2. The  $\alpha'$  is transformed from the  $\beta$  phase due to a very high cooling rate. For Ti-6Al-4V, a cooling rate of more than  $410\text{ }^{\circ}\text{C/s}$ , from the single  $\beta$  to the  $(\alpha+\beta)$  region, will induce  $\alpha'$  formations [24,25]. The  $\alpha'$  phase is commonly observed in Ti-6Al-4V alloy subject to rapid solidifications such as selective laser melting [26] and electron beam welding [27]. The width of the columnar prior  $\beta$  grains was measured in this study. Figure 2(a) illustrates an example of the width measurements. The image is overlaid with straight lines which are normal to the boundaries of the columnar structures and the intersections of the lines with grain boundaries were examined and used for width estimates. Different images from different specimen areas were measured to obtain statistical data. The average width of the columnar structure is about  $41.6\text{ }\mu\text{m}$  for this case (SF 36). This width is smaller to the columnar width reported by Al-Bermani et al. [8], 75 to  $150\text{ }\mu\text{m}$ .

Figures 2(b) and 3 illustrate typical microstructures of the Z-plane specimen, also from the SF 36 sample. Different from the microstructure of X-plane (Figure 2(a)), equiaxed thoroughly grains are noted. It can, thus, be concluded that the prior  $\beta$  grains are of a rod shape. Figures 3 shows higher magnification images of the Z-plane specimen from SEM, respectively; both  $\alpha$  and  $\beta$  phases can be identified. Upon cooling from the  $\beta$ -transus temperature, the initial  $\alpha$  that nucleates is “grain boundary”  $\alpha$  ( $\alpha_{\text{GB}}$ ) because of its location on prior  $\beta$  boundary. Eventually, the  $\beta$  boundaries will be replaced by  $\alpha_{\text{GB}}$  in a continuous fashion [22], as can be

noted from Figure 3(a). In addition, fine Widmanstätten ( $\alpha+\beta$ ) structures are shown inside of equiaxed grains, indicating a rapid cooling rate in EBAM. Widmanstätten ( $\alpha+\beta$ ) is a typical microstructure of Ti-6Al-4V alloy produced by EBAM, as can be clearly identified from high magnification images, Figure 3(b). In solid phase transformation, the prior  $\beta$  columnar grains are transformed into fine  $\alpha$  laths. The ( $\alpha+\beta$ ) structure is formed by diffusion controlled solid phase transformation, in which V diffuses into  $\beta$  while Al diffuses into  $\alpha$  [10]. Further, the classical  $\alpha$ -lath structure is surrounded by a very small amount of  $\beta$  in the  $\alpha$  boundaries. Compared with the wrought or cast Ti-6Al-4V, which shows coarse  $\alpha$  laths or equiaxed  $\alpha/\beta$  [1,16], EBAM Ti-6Al-4V parts show a finer  $\alpha$  phase. Stronger mechanical properties are expected for the finer microstructure [28,29]. Similar to the measurement method for the columnar width, intersections of the lines with prior  $\beta$  grain boundaries were marked and used for grain size estimates. The microstructural image was overlaid with several random lines, as shown in Figure 2(b). From the measurements, the estimated size of the equiaxed grains is 50.1  $\mu\text{m}$  in this case. The width of  $\alpha$  laths was also quantitatively analyzed using SEM images; an example is shown in Figure 3(b). The average thickness of  $\alpha$  laths is 1.1  $\mu\text{m}$  for this particular case, SF 36.

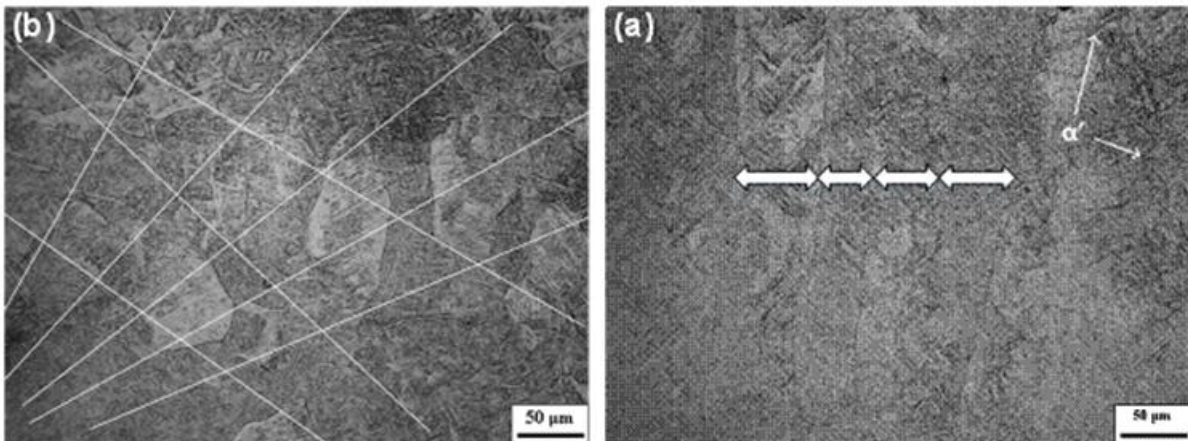


Figure 2. Microstructure from an EBAM sample (SF 36): (a) X-plane, and (b) Z-plane.

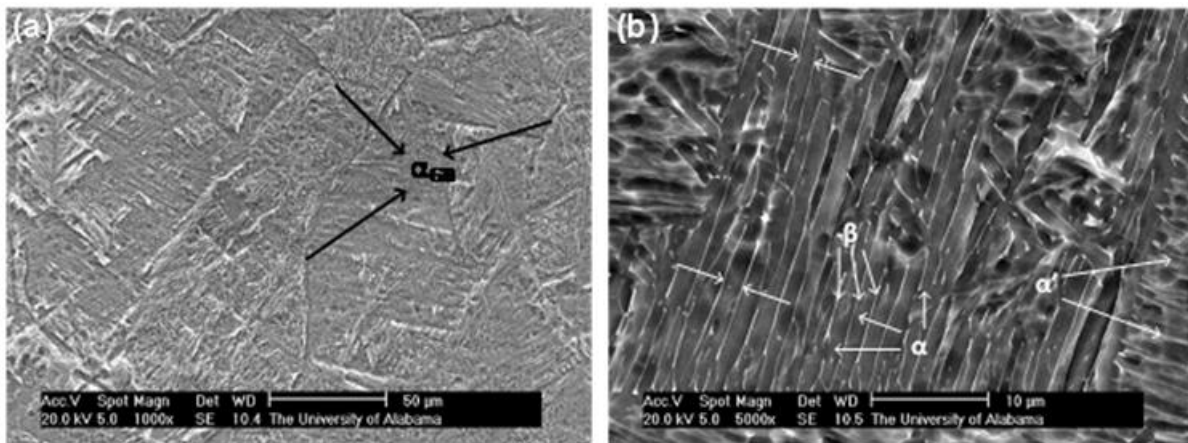


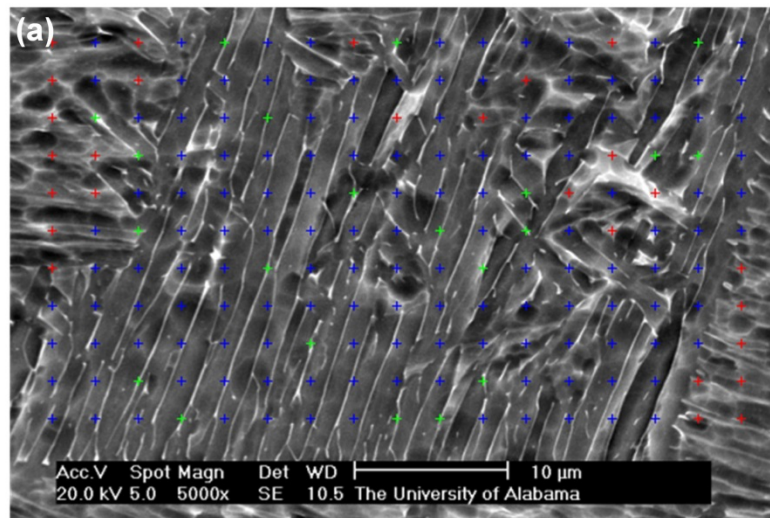
Figure 3. SEM images from Z-plane of an EBAM sample: (a) 1000  $\times$ , and (b) 5000  $\times$ .

The microstructures from other SF specimens (SF 20, SF 50 and SF 65) are also observed. The detailed microstructures could be checked from the previous study [19].

Generally, the width of columnar structure decreases with the increase of the scanning speed, 109.7  $\mu\text{m}$  at 214 mm/s vs. 37.1  $\mu\text{m}$  at 529 mm/s. The size of the equiaxed grains on the Z-plane has the same trend with the increase of the scanning speed: the SF 20 (lowest) sample has the largest grain size of 85.2  $\mu\text{m}$ , while the grain sizes for SF 36, SF 50 and SF 65 are similar, all less than 50  $\mu\text{m}$ . For the thickness of the  $\alpha$ -lath from different SF values, the SF 20 sample has the  $\alpha$ -lath thickness of 1.5  $\mu\text{m}$ , while the  $\alpha$ -lath thickness is around 1.0  $\mu\text{m}$  for other SF cases.

#### Phase Constitution Measurement and Phase Transformation Modeling

It is known that the mechanical properties (Young's modulus and hardness) of  $\alpha$ ,  $\beta$  and  $\alpha'$  are quite different and the mechanical properties of Ti-6Al-4V alloy may be calculated from the phase constitution of the alloy using the rule of mixtures [30]. The volume fraction of the phases ( $\alpha$ ,  $\beta$  and  $\alpha'$ ) may be determined using a regular grid of points overlaid onto the high magnification SEM image [31]. Dividing the number of points that lay within each phase by the total number of points gives an estimate of the phase fraction. Examples of SF 36 and SF 65 are shown in Figure 4; different colors represent different phases: blue for  $\alpha$ , green for  $\beta$  and red for  $\alpha'$ , respectively. For each SF sample, two high magnification images were used for a statistical study. The results of the phase fractions are shown in Figure 5. Generally, increasing the scanning speed, the fraction of  $\alpha$  decreases while the fraction of  $\alpha'$  increases noticeably. The trend of the volume fractions is correspondent to the theoretical study by the phase transformation kinetics. For  $\alpha$ , the phase transformation from  $\beta$  to  $\alpha$  is diffusional and time dependent. Thus, a slower cooling rate leads to the diffusion-controlled nucleation and growth process of secondary lamellae  $\alpha$  into the  $\beta$  grains; while a higher cooling rate provides a shorter time for the transformation and results in a smaller fractions of  $\alpha$ . For  $\beta$ , since it locates at the boundaries of  $\alpha$  laths, the volume fraction of  $\beta$  decreases with the decrease of  $\alpha$  when the scanning speed is increased. For  $\alpha'$  martensites, a high scanning speed results in a higher cooling rate which produces more martensites, i.e., the  $\alpha'$  fraction increases with the increase of the scanning speed.



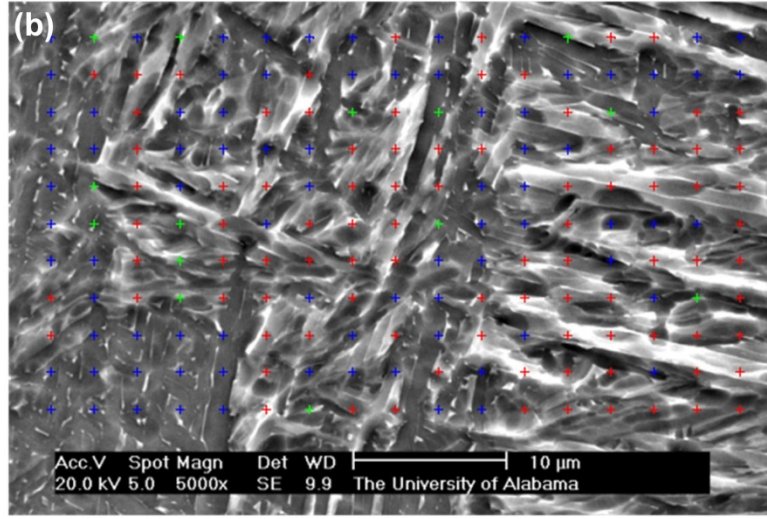


Figure 4. Examples of phase volume fraction measurements: (a) SF 36 and (b) SF 65.

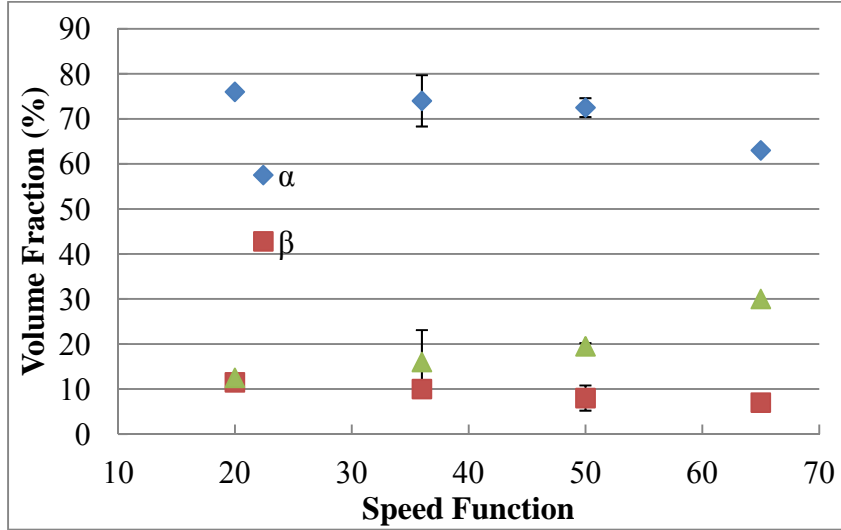


Figure 5. Result of volume fraction measurements with different SF values.

The microstructure depends strongly on the processing history. It is important to know the thermodynamics and kinetics of the phase transformations taking place during the EBAM process. One of the most effective methods is the Johnson-Mehl-Avrami (JMA) theory and it is valid for Ti-6Al-4V alloys [32]. Kelly studied the influence of cooling rates on the laser deposition process on Ti-6Al-4V alloy, in which a JMA model was used to predict the fraction of  $\alpha$  in the microstructure [22]. In an isothermal condition, the kinetics of the phase transformation is described by the JMA equation:

$$f(\alpha) = 1 - \exp(-kt^n), \quad (1)$$

where  $f(\alpha)$  is the volume fraction of the new phase at time  $t$ ,  $t$  is the time duration in seconds,  $k$  is the reaction rate constant, and  $n$  the Avrami, both  $k$  and  $n$  are dependent on the type of phase transformation and the grain growth. The  $n$  and  $k$  values are suggested as 1.15-1.6 and 0.033-

0.045 for Ti-6Al-4V alloys [33,34]. In the current study, the n and k used were as 1.5 and 0.04, respectively.

For a cooling rate higher than 410 °C/s, the  $\beta$  to  $\alpha$  transformation is suppressed and  $\beta$  transforms by a martensitic transformation into  $\alpha'$  martensite. The proportion of  $\beta$  transformed into martensite depends essentially on the undercooling below the  $M_s$  and is given by an empirical formula [35]:

$$f(\alpha') = f'(\beta) \{1 - \exp[-c(M_s - T)]\}, \quad (2)$$

where  $f'(\beta)$  is the volume fraction of the available  $\beta$  phase for martensitic transformation;  $M_s$  is the martensitic transformation starting temperature, and c is a material constant, whose value for Ti-6Al-4V is set as 0.015 [36].

To quantitatively estimate the phase fraction during solid-state phase transformation in EBAM, the cooling rates were first calculated from a 2D finite element (FE) thermal modeling. The detail of the FE model is introduced in a former research [4]. During the cooling in EBAM, a diffusion controlled transformation will take place and the  $\beta$  phase will progressively transform to  $\alpha$  phase as it cools from 980 °C (known as the  $\beta$ -transus temperature) [36] to  $M_s$  (725 °C). When the temperature is lower than  $M_s$ , whether the diffusion-controlled  $\beta$  to  $\alpha$  transformation or the martensitic transformation would take place was then governed based on the cooling rate. From the calculation of the thermal model simulations, the cooling rates from the four scanning speed cases are much higher than 410 °C/s. Hence, it means that the martensitic transformation will take place when the temperature is lower than  $M_s$ , and the diffusion-controlled transformation ( $\beta$  to  $\alpha$ ) stops. Figure 6 presents the phase fractions changed with the scanning speed and Figure 7 shows the difference of the phase volume fraction results between the analysis and the experiment. The estimated phase constitution is in a reasonable agreement with the experimental results. This indicates that the modeling approach is able to predict the microstructure evolution induced by EBAM processing of Ti-6Al-4V alloys.

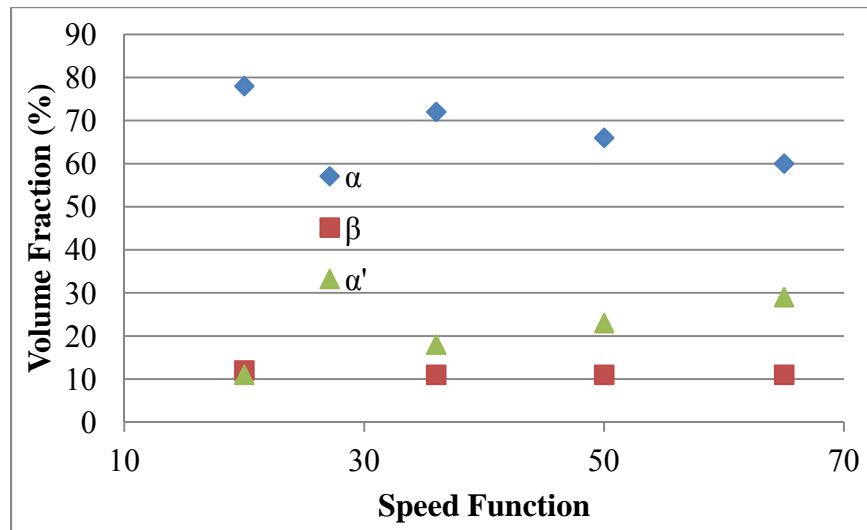


Figure 6. Theoretical analysis of volume fractions of different phases at different SF values.

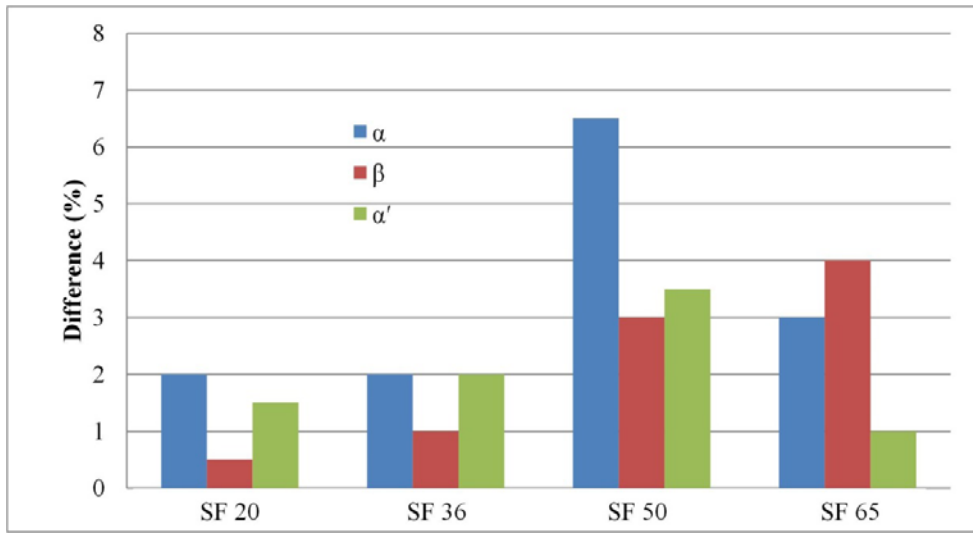


Figure 7. Differences in phase volume fractions between experimental and analytical results.

### Conclusions

In this study, four levels of the beam scanning speed, controlled by the speed function (SF) setting, were tested in building EBAM Ti-6Al-4V samples, which were subsequently used to prepare metallographic specimens for microstructural analysis. The effects of the beam speed on the build part microstructures were experimentally studied. A thermo-kinetic model coupling heat transfer and phase transformation kinetics, which predicts the phase constitution in Ti-6Al-4V by EBAM, was developed. In addition, the phase volume fractions were evaluated by experimental and computational methods. The major findings are summarized as follows.

- The side surface of the samples shows columnar prior  $\beta$  grains. With increasing the scanning speed, the width of the columnar grains tends to become smaller because of a higher cooling rate associated with the higher beam speed in EBAM.
- On the other hand, the scanning surface of the samples displays equiaxed grains. The grain size from the lowest-speed sample (SF 20) is much larger than that of samples from higher SF cases. The microstructure inside of equiaxed grains is Widmanstätten ( $\alpha+\beta$ ). In addition, increasing the scanning speed will also result in finer  $\alpha$ -lath.
- From the experimental study of the phase constitution, increasing the scanning speed results in the increase of the  $\alpha'$  martensite and the decrease of  $\alpha$ . The variation of the phase volume fractions at different scanning speeds could be attributed to the different cooling rates during solid phase transformation.
- The cooling rate and the temperature history from the EBAM thermal model are incorporated well into the phase transformation modeling. The result of the phase transformation model is consistent with the experimental results.

### Acknowledgements

The materials presented in this paper are supported by NASA, under award No. NNX11AM11A. The author XG also acknowledges the fellowship awarded by the AL EPSCoR GRSP to conduct this study.

### **References**

- [1] Murr, L.E., Esquivel, E.V., Quinones, S.A., Gaytan, S.M., Lopez, M.I., Martinez, E.Y., Medina, F., Hernandez, D.H., Martinez, E., Martinez, J.L., Stafford, S.W., Brown, D.K., Hoppe, T., Meyers, W., Lindhe, U., and Wicker, R.B., 2009, "Microstructures and mechanical properties of electron beam-rapid manufactured Ti-6Al-4V biomedical prototypes compared to wrought Ti-6Al-4V," *Materials Characterization*, 60, pp. 96-105.
- [2] Gong, X. and Chou, K., 2013, "Characterizations of sintered Ti-6Al-4V powders in electron beam additive manufacturing," *Proceedings of the ASME 2013 International Manufacturing Science and Engineering Conference*, Madison, WI, 2013, pp. V001T01A002.
- [3] Zäh, M.F. and Lutzmann, S., 2010, "Modelling and simulation of electron beam melting," *Production Engineering*, 4, pp. 15-23.
- [4] Gong, X., Cheng, B., Price, S., and Chou, K., 2013, "Powder-bed electron-beam-melting additive manufacturing: powder characterization, process simulation and metrology," *ASME District F- ECTC 2013: Early Career Technical Conference*, Birmingham, AL, 12, pp. 59-66.
- [5] Price, S., Cooper, K., and Chou, K., 2012, "Evaluations of temperature measurements by near-infrared thermography in powder-based electron-beam additive manufacturing," *Solid Freeform Fabrication Symposium*, Austin, TX, pp. 761-773.
- [6] Koike, M., Martinez, K., Guo, L., Chahine, G., Kovacevic, R., and Okabe, T., 2011, "Evaluation of titanium alloy fabricated using electron beam melting system for dental applications," *Journal of Materials Processing Technology*, pp. 1400-1408.
- [7] Cooke, A.L. and Soons, J.A., 2010, "Variability in the geometric accuracy of additively manufactured test parts," *Solid Freeform Fabrication Symposium*, Austin, TX, pp. 1-12.
- [8] Al-Bermani, S.S., Blackmore, M.L., Zhang, W., and Todd, I., 2010, "The origin of microstructural diversity, texture, and mechanical properties in electron beam melted Ti-6Al-4V," *Metallurgical and Materials Transactions A*, 41A, pp. 3422-3434.
- [9] Safdar, A., Wei, L.Y., Snis, A., and Lai, Z., 2012, "Evaluation of microstructural development in electron beam melted Ti-6Al-4V," *Materials Characterization*, 65, pp. 8-15.
- [10] Facchini, L., Magalini, E., Robotti, P., and Molinari, A., 2009, "Microstructure and mechanical properties of Ti-6Al-4V produced by electron beam melting of pre-alloyed powders," *Rapid Prototyping Journal*, 15, pp. 171-178.
- [11] Christensen, A., Kircher, R., and Lippincott, A., 2007, "Qualification of electron beam melted (EBM) Ti6Al4V-ELI for orthopaedic applications," *Proceedings of the Materials and Processes for Medical Devices Conference*, Palm Desert, CA, pp. 48-53.
- [12] Murr, L.E., Gaytan, S.M., Medina, F., Martinez, E., Martinez, J.L., Hernandez, D.H., Machado, B.I., Ramirez, D.A., and Wicker, R.B., 2010, "Characterization of Ti-6Al-4V open cellular foams fabricated by additive manufacturing using electron beam melting," *Materials Science and Engineering A*, 527, pp. 1861-1868.
- [13] Gong, X., Anderson, T., and Chou, K., 2014, "Review on powder-based electron beam additive manufacturing technology," *Proceedings of the ASME/ISCIE 2012 International Symposium on Flexible Automation*, pp. 507-515.

- [14] Murr, L.E., Gaytan, S.M., Medina, F., Martinez, E., Hernandez, D.H., Martinez, L., Lopez, M.I., Wicker, R.B., and Collins, S., 2009, "Effect of build parameters and build geometries on residual microstructures and mechanical properties of Ti-6Al-4V components built by electron beam melting (EBM)," Solid Freeform Fabrication Symposium, Austin, TX, pp. 374-397.
- [15] Bontha, S., Klingbeil, N.W., Kobryn, P.A., and Fraser, H.L., 2009, "Effects of process variables and size-scale on solidification microstructure in beam-based fabrication of bulky 3D structures," Materials Science and Engineering A, 513-514, pp. 311-318.
- [16] Murr, L.E., Quinones, S.A., Gaytan, S.M., Lopez, M.I., Rodela, A., Martinez, E.Y., Hernandez, D.H., Martinez, E., Medina, F., and Wicker, R.B., 2009, "Microstructure and mechanical behavior of Ti-6Al-4V produced by rapid-layer manufacturing, for biomedical applications," Journal of the Mechanical Behavior of Biomedical Materials, 2, pp. 20-32.
- [17] Jamshidinia, M., Kong, F., and Kovacevic, R., 2013, "The coupled CFD-FEM model of electron beam melting (EBM)," ASME District F- ECTC 2013: Early Career Technical Conference, Birmingham, AL, 12, pp. 163-171.
- [18] Mahale, T.R., 2009, "Electron beam melting of advanced materials and structures," Ph. D. Dissertation, North Carolina State University, Raleigh, NC.
- [19] Gong, X., Lydon, J., Cooper, K., and Chou, K., 2014, "Beam Speed Effects on Ti-6Al-4V Microstructures in Electron Beam Additive Manufacturing," Journal of Materials Research, accepted for publication, June 2014.
- [20] Wang, K., Zeng, W., Shao, Y., Zhao, Y., and Zhou, Y., 2009, "Quantification of microstructural features in titanium alloys based on stereology," Rare Metal Materials and Engineering 38, pp. 398-403.
- [21] Collins, P.C., Welk, B., Searles, T., Tiley, J., Russ, J.C., and Fraser H.L., 2009, "Development of methods for the quantification of microstructural features in  $\alpha+\beta$ -processed  $\alpha/\beta$  titanium alloys," Materials Science and Engineering: A 508, 1, pp. 174-182.
- [22] Kelly, S.M., 2004, "Thermal and microstructure modeling of metal deposition processes with application to Ti-6Al-4V," Ph. D. Dissertation, Virginia Polytechnic Institute and State University, Blacksburg, VA.
- [23] Wu, X., Liang, J., Mei, J., Mitchell, C., Goodwin, P.S., and Voice, W., 2004, "Microstructures of laser-deposited Ti-6Al-4V," Materials and Design, 25, pp. 137-144.
- [24] Ahmed, T. and Rack, H.J., 1998, "Phase transformations during cooling in  $\alpha + \beta$  titanium alloys," Materials Science and Engineering A, 243, pp. 206-211.
- [25] Gong, X., Lydon, J., Cooper, K., and Chou, K., "Characterization of Ti-6Al-4V powder in electron beam melting additive manufacturing," Additive Manufacturing with Powder Metallurgy (AMPM 2014), Orlando, FL, May 18-20, 2014 (AMPM2014-1149).
- [26] Baufeld, B., Brandl, E., and Biest, O.v.d., 2011, "Wire based additive layer manufacturing: Comparison of microstructure and mechanical properties of Ti-6Al-4V components fabricated by laser-beam deposition and shaped metal deposition," Journal of Materials Processing Technology, 211, pp. 1146-1158.
- [27] Lu, W., Shi, Y., Lei, Y., and Li, X., 2012, "Effect of electron beam welding on the microstructures and mechanical properties of thick TC4-DT alloy," Materials Design, 34, pp. 509-515.
- [28] Gong, X., Li, H., Kang, S.B., Cho, J.H., and Li, S., 2010, "Microstructure and mechanical properties of twin-roll cast Mg-4.5Al-1.0Zn alloy sheets processed by differential speed rolling," Materials and Design, 31(3), pp. 1581-1587.

- [29] Gong, X., Kang, S.B., Li, S., and Cho, J.H., 2009, "Enhanced plasticity of twin-roll cast ZK60 magnesium alloy through differential speed rolling," *Materials and Design*, 30(9), pp. 3345-3350.
- [30] Crespo, A., 2011, "Modelling of Heat Transfer and Phase Transformations in the Rapid Manufacturing of Titanium Components," *Convection and Conduction Heat Transfer*, edited by Amimul Ahsan, pp. 315-340.
- [31] Tiley, J., Searles, T., Lee, E., Kar, S., Banerjee, R., Russ, J.C., and Fraser, H.L., 2004, Quantification of microstructural features in  $\alpha/\beta$  titanium alloys," *Materials Science and Engineering: A*, 372(1), pp. 191-198.
- [32] Charles, C., 2008, "Modelling microstructure evolution of weld deposited Ti-6Al-4V," Thesis, Luleå University of Technology, Luleå, Sweden.
- [33] Malinov, S., Guo, Z., Sha, W., and Wilson, A., 2001, Differential scanning calorimetry study and computer modeling of  $\beta$  to  $\alpha$  phase transformation in a Ti6Al4V alloy," *Metallurgical and Materials Transactions A*, 32(4), pp. 879-887.
- [34] Fan, Y., Cheng, P., Yao, Y.L., Yang, Z., and Egland, K., 2005, "Effect of phase transformations on laser forming of Ti-6Al-4V alloy," *Journal of Applied Physics*, 98(1), pp. 013518.
- [35] Elmer, J.W., Palmer, T.A., Babu, S.S., Zhang, W., and Debroy, T., 2004, "Phase transformation dynamics during welding of Ti-6Al-4V," *Journal of Applied Physics*, 95, pp. 8327-8339.
- [36] Crespo, A., Deus, A., and Vilar, R., 2009, "Modeling of Phase Transformations and Internal Stresses in Laser Powder Deposition," *Proceedings of SPIE*, 7131, pp. 713120-3.